

Excitation functions of kinetic freeze-out temperature and transverse flow velocity in proton-proton collisions

Li-Li Li, Fu-Hu Liu*

*Institute of Theoretical Physics and State Key Laboratory of Quantum Optics and Quantum Optics Devices,
Shanxi University, Taiyuan, Shanxi 030006, China*

Abstract: Transverse momentum spectra of negative and positive pions produced at mid-(pseudo)rapidity in inelastic or non-single-diffractive proton-proton (pp) collisions over a center-of-mass energy, \sqrt{s} , range from a few GeV to above 10 TeV are analyzed by the blast-wave model with Boltzmann-Gibbs (Tsallis) statistics. The model results are well fitting to the experimental data measured by the NA61/SHINE, PHENIX, STAR, ALICE, and CMS Collaborations. In a particular superposition with Hagedorn function, both excitation functions of kinetic freeze-out temperature (T_0) of emission source and transverse flow velocity (β_T) of produced particles obtained from a given selection in the blast-wave model with Boltzmann-Gibbs statistics have a hill at $\sqrt{s} \approx 10$ GeV, a drop at dozens of GeV, and then an increase from dozens of GeV to above 10 TeV. Nevertheless, both excitation functions of T_0 and β_T obtained in the blast-wave model with Tsallis statistics do not show such a complex structure, but a very low hill. In another selection for the parameters or in the superposition with the usual step function, T_0 and β_T increase generally slightly from a few GeV to above 10 TeV.

Keywords: Excitation function of kinetic freeze-out temperature, excitation function of transverse flow velocity, proton-proton collisions

PACS: 14.40.Aq, 13.85.Hd, 13.75.Cs

1 Introduction

Chemical and thermal or kinetic freeze-outs are two of important stages of system evolution in high energy collisions. The excitation degrees of interacting system at the two stages are possibly different from each other. To describe different excitation degrees of interacting system at the two stages, one can use chemical and kinetic freeze-out temperatures respectively. Generally, at the stage of chemical freeze-out, the ratios of different types of particles are no longer changed, and the chemical freeze-out temperature can be obtained from the ratios of different particles in the framework of thermal model [1–3]. At the stage of kinetic freeze-out, the transverse momentum spectra of different particles are no longer changed, and the dissociation temperature [4] or kinetic freeze-out temperature can be obtained from the transverse momentum spectra according to the hydrodynamical model [4] and the subsequent blast-wave model with Boltzmann-Gibbs statistics [5–7] and with Tsallis statistics [8–10].

It should be pointed out that the transverse momentum spectra even though in narrow range contain both the contributions of random thermal motion and transverse flow of particles. The former and the latter reflect the excitation degree and collective expansion of the in-

teracting system (or emission source) respectively. To extract the kinetic freeze-out temperature from transverse momentum spectra, we have to exclude the contribution of transverse flow, that is, we have to disengage the random thermal motion and transverse flow. There are more than one methods to disengage the two issues [4]. The simplest and easiest method is to use the blast-wave model with Boltzmann-Gibbs statistics [5–7] and with Tsallis statistics [8–10] to analyze the transverse momentum spectra, though other method such as the alternative method [6, 11–17] can obtain similar results [18].

The early blast-wave model is based on the Boltzmann-Gibbs statistics [5–7]. An alternative blast-wave model is used due to the Tsallis statistics [8–10]. Both types of blast-wave model can be used to disengage the random thermal motion and transverse flow. Then, the kinetic freeze-out temperature of interacting system and transverse flow velocity of light flavor particles can be extracted. Most of light flavor particles are produced in soft excitation process and have narrow transverse momentum range up to $2\sim 3$ GeV/ c . A few part of light flavor particles are produced in hard scattering process and have higher transverse momenta. Generally, heavy flavor particles are produced via hard

*E-mail: fuhuli@163.com; fuhuli@sxu.edu.cn

scattering process. From the point of view of disengaging or extraction, particles produced in hard scattering process are not needed to consider by us.

The excitation function of the kinetic freeze-out temperature, that is, its dependence on collision energy, are very interesting for us to study the properties of high energy collisions. Although there are many similar studies on this topic, the results seem to be inconsistent. For example, over a center-of-mass energy, $\sqrt{s_{NN}}$, range from a few GeV to a few TeV, the excitation function of the kinetic freeze-out temperature in gold-gold (Au-Au) and lead-lead (Pb-Pb) collisions initially increases and then inconsistently saturates [19, 20], increases [21], or decreases [22, 23] with the increase of collision energy. On the contrary, the excitation function of the chemical freeze-out temperature shows initially increases and then consistently saturates with collision energy [1–4]. Comparatively, as the basic processes in nucleus-nucleus collisions, proton-proton (pp or $p-p$) collisions are minor in the study of the mentioned excitation functions.

It is worth to study the excitation function of the kinetic freeze-out temperature in pp collisions and to judge its tendency at the LHC. In this paper, by using the blast-wave model with Boltzmann-Gibbs statistics [5–7] and with Tsallis statistics [8–10], we study the excitation functions of some concerned quantities in inelastic (INEL) or non-single-diffractive (NSD) pp collisions which are closer to peripheral nuclear collisions comparing with central nuclear collisions. The experimental transverse momentum spectra of negative and positive pions (π^- and π^+) measured at the mid-rapidity by the NA61/SHINE Collaboration [24] at the the Super Proton Synchrotron (SPS) and its beam energy scan (BES) program, the PHENIX [25] and STAR [6] Collaborations at the Relativistic Heavy Ion Collider (RHIC), as well as the ALICE [26] and CMS [27, 28] Collaborations at the Large Hadron Collider (LHC) are analyzed.

The remainder of this paper is structured as follows. The formalism and method are shortly described in Section 2. Results and discussion are given in Section 3. In Section 4, we summarize our main observations and conclusions.

2 Formalism and method

There are two main processes of particle productions, namely the soft excitation process and the hard scattering process, in high energy collisions. For the soft excitation process, the model used in the present work is the blast-wave model [5–10] that has wide applications in particle productions. The model is based on two types of statistics. One is the Boltzmann-Gibbs statistics [5–7] and another one is the Tsallis statistics [8–10]. As an application of the model, we present directly its for-

malisms in the following. Although the model has abundant connotations, we focus only our attention on the formalism of transverse momentum (p_T) distribution in which the kinetic freeze-out temperature (T_0) and mean transverse flow velocity (β_T) are included.

We are interested in the blast-wave model with Boltzmann-Gibbs statistics in its original form. According to refs. [5–7], the blast-wave model with Boltzmann-Gibbs statistics results in the probability density distribution of p_T to be

$$f_1(p_T) = \frac{1}{N} \frac{dN}{dp_T} = C_1 p_T m_T \int_0^R r dr \times I_0 \left[\frac{p_T \sinh(\rho)}{T_0} \right] K_1 \left[\frac{m_T \cosh(\rho)}{T_0} \right], \quad (1)$$

where C_1 is the normalized constant, $m_T = \sqrt{p_T^2 + m_0^2}$ is the transverse mass, m_0 is the rest mass, r is the radial coordinate in the thermal source, R is the maximum r which can be regarded as the transverse size of participant in the case of neglecting the expansion of source, r/R is the relative radial position which has in fact more meanings than r and R themselves, I_0 and K_1 are the modified Bessel functions of the first and second kinds respectively, $\rho = \tanh^{-1}[\beta(r)]$ is the boost angle, $\beta(r) = \beta_S (r/R)^{n_0}$ is a self-similar flow profile, β_S is the flow velocity on the surface, and $n_0 = 2$ is used in the original form [5]. There is the relation between β_T and $\beta(r)$. As a mean of $\beta(r)$, $\beta_T = (2/R^2) \int_0^R r \beta(r) dr = 2\beta_S / (n_0 + 2)$.

We are also interested in the blast-wave model with Tsallis statistics in its original form. According to ref. [8–10], the blast-wave model with Tsallis statistics results in the p_T distribution to be

$$f_2(p_T) = \frac{1}{N} \frac{dN}{dp_T} = C_2 p_T m_T \int_{-\pi}^{\pi} d\phi \int_0^R r dr \left\{ 1 + \frac{q-1}{T_0} [m_T \cosh(\rho) - p_T \sinh(\rho) \cos(\phi)] \right\}^{-1/(q-1)}, \quad (2)$$

where C_2 is the normalized constant, q is an entropy index that characterizes the degree of non-equilibrium, ϕ denotes the azimuthal angle, and $n_0 = 1$ is used in the original form [8]. Because of n_0 being an insensitive quantity, the results corresponding to $n_0 = 1$ and 2 for the blast-wave model with Boltzmann-Gibbs or Tsallis statistics are harmonious [18]. In addition, the index $-1/(q-1)$ used in Eq. (2) can be replaced by $-q/(q-1)$ due to q being very close to 1. This substitution results in a small and negligible difference in the Tsallis distribution [29, 30].

For a not too wide p_T spectrum, the above two equations can be used to describe the p_T spectrum and to extract the kinetic freeze-out temperature and transverse flow velocity. For a wide p_T spectrum, we have

to consider the contribution of hard scattering process. According to the quantum chromodynamics (QCD) calculus [31–33], the contribution of hard scattering process is parameterized to be an inverse power-law

$$f_H(p_T) = \frac{1}{N} \frac{dN}{dp_T} = Ap_T \left(1 + \frac{p_T}{p_0}\right)^{-n} \quad (3)$$

which is the Hagedorn function [34, 35], where p_0 and n are free parameters, and A is the normalization constant related to the free parameters. In literature [36], [37–41], and [42], there are respectively modified Hagedorn functions

$$f_H(p_T) = \frac{1}{N} \frac{dN}{dp_T} = A \frac{p_T^2}{m_T} \left(1 + \frac{p_T}{p_0}\right)^{-n}, \quad (4)$$

$$f_H(p_T) = \frac{1}{N} \frac{dN}{dp_T} = Ap_T \left(1 + \frac{p_T^2}{p_0^2}\right)^{-n}, \quad (5)$$

and

$$f_H(p_T) = \frac{1}{N} \frac{dN}{dp_T} = A \left(1 + \frac{p_T^2}{p_0^2}\right)^{-n}, \quad (6)$$

where the three normalization constants A , free parameters p_0 , and free parameters n are severally different, though the same symbols are used to avoid trivial expression.

The experimental p_T spectrum distributed in a wide range can be described by a superposition of the soft excitation and hard scattering processes. We have

$$f_0(p_T) = kf_S(p_T) + (1 - k)f_H(p_T), \quad (7)$$

where k denotes the contribution fraction of the soft excitation process, and $f_S(p_T)$ denotes one of Eqs. (1) and (2). As for the four $f_H(p_T)$, we are inclined to the first one due to its more applications. According to Hagedorn's model [34], we may also use the usual step function to superpose the two functions. That is

$$f_0(p_T) = A_1\theta(p_1 - p_T)f_S(p_T) + A_2\theta(p_T - p_1)f_H(p_T), \quad (8)$$

where A_1 and A_2 are constants which result in the two components to be equal to each other at $p_T = p_1 \approx 2 \sim 3$ GeV/ c . The contribution fraction of the soft process in Eq. (8) is $k = \int_0^{p_1} A_1 f_S(p_T) dp_T$.

In some cases, the contribution of resonance production for pions in very-low p_T range cannot be neglected. We have to use a very-soft component for the p_T range from 0 to 0.2~0.3 GeV/ c . Let k_{VS} and k_S denote the contribution fractions of the very-soft and soft processes respectively. Eq. (7) is revised to

$$f_0(p_T) = k_{VS}f_{VS}(p_T) + k_S f_S(p_T) + (1 - k_{VS} - k_S)f_H(p_T), \quad (9)$$

where $f_{VS}(p_T)$ denotes one of Eqs. (1) and (2) as $f_S(p_T)$, but having smaller parameter values comparing with $f_S(p_T)$. Anyhow, both the very-soft and soft processes are belong to the soft process. Correspondingly, Eq. (8) is revised to

$$f_0(p_T) = A_1\theta(p_1 - p_T)f_{VS}(p_T) + A_2\theta(p_T - p_1)\theta(p_2 - p_T)f_S(p_T) + A_3\theta(p_T - p_2)f_H(p_T), \quad (10)$$

where A_1 , A_2 , and A_3 are constants which result in the two contiguous components to be equal to each other at $p_T = p_1$ and $p_T = p_2$.

The above two types of superpositions [Eqs. (7) and (8)] have different treatments for the soft and hard components in the whole p_T range. Eq. (7) means that the soft component contributes in a range from 0 up to 2~3 GeV/ c or a little more. The hard component contributes in the whole p_T range, though the main contributor in the low p_T region is the soft component and the sole contributor in the high p_T region is the hard component. Eq. (8) shows that the soft component contributes in a range from 0 up to p_1 , and the hard component contributes in a range from p_1 up to the maximum. The boundary of the contributions of soft and hard components is p_1 . There is no mixed region for the two components in Eq. (8).

In the case of including only the soft component, Eqs. (7) and (8) are the same. In the case of including both the soft and hard components, their common parameters such as T_0 , β_T , p_0 , and n should be severally different from each other. To avoid large differences, we should select the experimental data in a narrow p_T range. In addition, most experimental data in the very-low p_T region are not available. The very-soft component in Eqs. (9) and (10) are in fact negligible. Thus, in the case of neglecting the very-soft component, Eqs. (9) and (10) are degenerated to Eqs. (7) and (8) respectively. Firstly, we shall use Eq. (7) to extract the related parameters, where $f_S(p_T)$ and $f_H(p_T)$ are exactly Eqs. (1) or (2) and (3) respectively. Regardless of Eq. (1) or (2) is regarded as $f_S(p_T)$, the situation is similar due to Eqs. (1) and (2) being harmonious in trends of parameters [18], though one more parameter (the entropy index q) is needed in Eq. (2). Secondly, we shall use Eq. (8) to extract the related parameters as comparisons with those from Eqs. (7).

3 Results and discussion

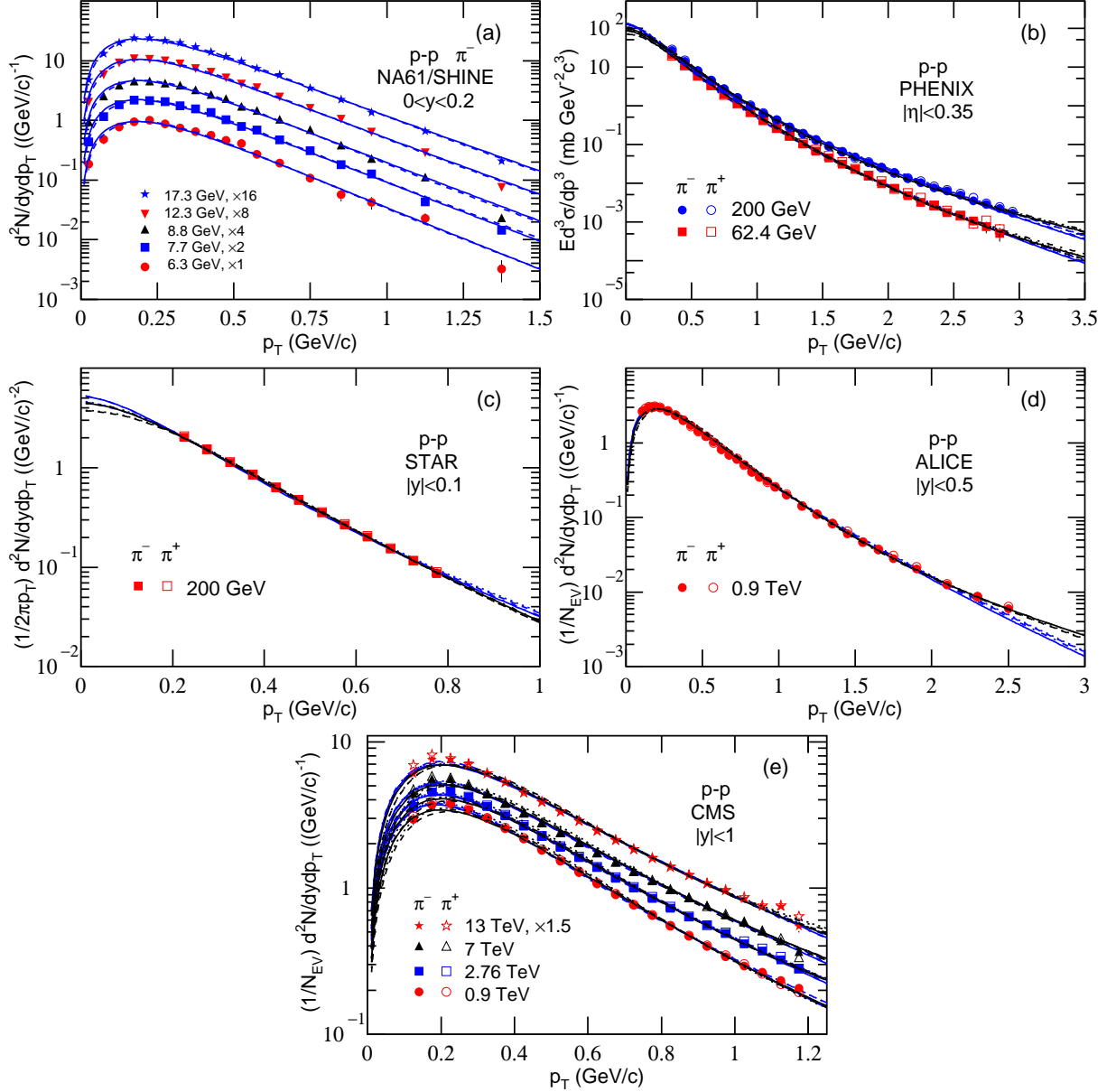


Fig. 1. Transverse momentum spectra of π^- and π^+ produced at mid-(pseudo)rapidity in pp collisions at high energies, where the mid-(pseudo)rapidity intervals and energies are marked in the panels. The symbols presented in panels (a)–(e) represent the data of NA61/SHINE [24], PHENIX [25], STAR [6], ALICE [26], and CMS [27, 28] Collaborations, respectively, where in panel (a) only the spectra of π^- are available, and panel (c) is for NSD events and other panels are for INEL events. In some cases, different amounts marked in the panels are used to scale the data for clarity. The blue solid (dotted) curves are our results for π^- (π^+) spectra fitted by Eq. (7) through Eqs. (1) and (3), and the blue dashed (dot-dashed) curves are our results for π^- (π^+) spectra fitted by Eq. (7) through Eqs. (2) and (3), by the first set of parameter values. The results by the second set of parameters (if available) are presented by the black curves.

Figure 1 shows the transverse momentum spectra of π^- and π^+ produced at mid-(pseudo)rapidity in pp collisions at high center-of-mass energies, where different mid-(pseudo)rapidity (y or η) intervals and energies (\sqrt{s}) are marked in the panels. Different forms of the spectra are used due to different Collaborations, where

N , E , p , σ , and N_{EV} denote the particle number, energy, momentum, cross-section, and event number, respectively. The closed and open symbols presented in panels (a)–(e) represent the data of π^- and π^+ measured by the NA61/SHINE [24], PHENIX [25], STAR [6], ALICE [26], and CMS [27, 28] Collaborations, respectively,

Table 1. Values of free parameters (T_0 , β_T , k , p_0 , and n), normalization constant (N_0), χ^2 , and dof corresponding to the solid (dotted) curves for π^- (π^+) spectra in Fig. 1 in which different data are measured in different mid-(pseudo)rapidity intervals at different energies by different Collaborations. The values presented in terms of value₁/value₂ denote respectively the first and second sets of parameter values in Eq. (7) through Eqs. (1) and (3) in which $k \neq 1$.

Collab.	\sqrt{s} (GeV)	Part.	T_0 (MeV)	β_T (c)	k	p_0 (GeV/c)	n	N_0	χ^2	dof
NA61/ SHINE	6.3	π^-	108 ± 5	0.30 ± 0.02	1	—	—	0.08 ± 0.01	21	15
	7.7	π^-	109 ± 5	0.31 ± 0.02	1	—	—	0.10 ± 0.01	34	15
	8.8	π^-	110 ± 5	0.31 ± 0.02	1	—	—	0.10 ± 0.01	73	15
	12.3	π^-	111 ± 6	0.32 ± 0.02	1	—	—	0.12 ± 0.01	59	15
	17.3	π^-	112 ± 6	0.33 ± 0.02	1	—	—	0.13 ± 0.01	26	15
PHENIX	62.4	π^-	96 ± 5/114 ± 6	0.27 ± 0.01/0.34 ± 0.02	0.66 ± 0.01/0.98 ± 0.01	3.60 ± 0.18/6.06 ± 0.30	19.23 ± 0.96/18.63 ± 0.93	21.55 ± 1.08/18.96 ± 0.95	7/28	20
		π^+	96 ± 5/114 ± 6	0.27 ± 0.01/0.34 ± 0.02	0.66 ± 0.01/0.98 ± 0.01	3.63 ± 0.18/6.07 ± 0.30	19.03 ± 0.95/18.63 ± 0.93	20.81 ± 1.04/18.57 ± 0.93	11/11	20
	200	π^-	100 ± 5/116 ± 5	0.30 ± 0.02/0.36 ± 0.02	0.62 ± 0.01/0.96 ± 0.02	4.19 ± 0.21/6.45 ± 0.32	19.01 ± 0.95/18.01 ± 0.90	23.98 ± 1.20/22.77 ± 1.14	26/21	21
		π^+	100 ± 5/115 ± 5	0.30 ± 0.02/0.35 ± 0.02	0.62 ± 0.01/0.96 ± 0.02	4.21 ± 0.21/6.46 ± 0.32	19.01 ± 0.95/18.00 ± 0.90	24.41 ± 1.22/24.41 ± 1.22	54/26	21
STAR	200	π^-	98 ± 6/112 ± 5	0.29 ± 0.02/0.34 ± 0.02	0.61 ± 0.03/0.98 ± 0.02	4.01 ± 0.20/6.00 ± 0.30	19.21 ± 0.96/18.61 ± 0.93	0.27 ± 0.01/0.92 ± 0.05	76/3	6
		π^+	99 ± 6/112 ± 5	0.29 ± 0.02/0.34 ± 0.02	0.60 ± 0.03/0.98 ± 0.02	4.01 ± 0.20/6.00 ± 0.30	19.21 ± 0.96/18.61 ± 0.93	0.27 ± 0.01/0.27 ± 0.01	96/4	6
ALICE	900	π^-	101 ± 5/116 ± 6	0.31 ± 0.02/0.36 ± 0.02	0.63 ± 0.02/0.94 ± 0.02	4.39 ± 0.22/6.81 ± 0.34	18.89 ± 0.94/17.35 ± 0.87	1.47 ± 0.07/1.47 ± 0.07	38/126	27
		π^+	101 ± 5/116 ± 6	0.31 ± 0.02/0.35 ± 0.02	0.63 ± 0.02/0.95 ± 0.02	4.42 ± 0.22/6.96 ± 0.35	18.81 ± 0.94/17.35 ± 0.87	1.47 ± 0.07/1.47 ± 0.07	49/137	27
CMS	900	π^-	101 ± 5/115 ± 6	0.31 ± 0.02/0.35 ± 0.02	0.63 ± 0.03/0.91 ± 0.02	4.43 ± 0.22/7.08 ± 0.35	18.71 ± 0.93/17.13 ± 0.87	3.65 ± 0.18/3.49 ± 0.17	24/62	16
		π^+	101 ± 5/115 ± 5	0.31 ± 0.02/0.35 ± 0.02	0.63 ± 0.03/0.92 ± 0.02	4.43 ± 0.22/7.04 ± 0.35	18.71 ± 0.93/17.16 ± 0.86	3.70 ± 0.19/3.55 ± 0.18	16/59	16
	2760	π^-	103 ± 6/116 ± 4	0.33 ± 0.02/0.36 ± 0.02	0.63 ± 0.03/0.90 ± 0.02	4.68 ± 0.23/7.80 ± 0.39	18.41 ± 0.92/16.45 ± 0.82	4.47 ± 0.22/4.31 ± 0.22	34/70	16
		π^+	102 ± 6/116 ± 5	0.33 ± 0.02/0.36 ± 0.02	0.63 ± 0.04/0.91 ± 0.02	4.69 ± 0.23/7.90 ± 0.39	18.39 ± 0.92/16.35 ± 0.82	4.55 ± 0.23/4.43 ± 0.22	35/74	16
	7000	π^-	104 ± 5/117 ± 6	0.34 ± 0.02/0.37 ± 0.02	0.62 ± 0.03/0.89 ± 0.02	4.79 ± 0.24/8.00 ± 0.40	18.21 ± 0.91/16.13 ± 0.81	5.50 ± 0.27/5.49 ± 0.27	48/67	16
		π^+	103 ± 5/116 ± 4	0.34 ± 0.02/0.36 ± 0.02	0.61 ± 0.04/0.89 ± 0.02	4.80 ± 0.24/8.20 ± 0.41	18.21 ± 0.91/16.00 ± 0.80	5.54 ± 0.28/5.52 ± 0.28	55/70	16
	13000	π^-	105 ± 5/117 ± 5	0.35 ± 0.02/0.37 ± 0.02	0.61 ± 0.03/0.89 ± 0.02	4.90 ± 0.24/8.30 ± 0.41	18.11 ± 0.90/15.99 ± 0.80	5.07 ± 0.25/5.07 ± 0.25	30/28	16
		π^+	104 ± 5/117 ± 5	0.34 ± 0.02/0.36 ± 0.02	0.64 ± 0.04/0.88 ± 0.02	5.00 ± 0.25/8.99 ± 0.43	18.00 ± 0.90/15.59 ± 0.78	5.12 ± 0.26/5.15 ± 0.26	36/42	16

27

Table 2. Values of free parameters (T_0 , β_T , q , k , p_0 , and n), normalization constant (N_0), χ^2 , and dof corresponding to the dashed (dot-dashed) curves for π^- (π^+) spectra in Fig. 1 in which different data are measured in different mid-(pseudo)rapidity intervals at different energies by different Collaborations. The values presented in terms of value₁/value₂ denote respectively the first and second sets of parameter values in Eq. (7) through Eqs. (2) and (3) in which $k \neq 1$.

Collab.	\sqrt{s} (GeV)	Part.	T_0 (MeV)	β_T (c)	q	k	p_0 (GeV/c)	n	N_0	χ^2	dof
NA61/ SHINE	6.3	π^-	81 ± 4	0.19 ± 0.01	1.05 ± 0.002	1	—	—	0.08 ± 0.01	12	14
	7.7	π^-	81 ± 4	0.20 ± 0.01	1.06 ± 0.002	1	—	—	0.10 ± 0.01	13	14
	8.8	π^-	83 ± 4	0.20 ± 0.01	1.05 ± 0.002	1	—	—	0.10 ± 0.01	24	14
	12.3	π^-	84 ± 4	0.21 ± 0.01	1.06 ± 0.002	1	—	—	0.12 ± 0.01	14	14
	17.3	π^-	85 ± 4	0.21 ± 0.01	1.06 ± 0.002	1	—	—	0.13 ± 0.01	5	14
PHENIX	62.4	π^-	78 ± 4/86 ± 4	0.18 ± 0.01/0.21 ± 0.01	1.04 ± 0.01/1.06 ± 0.01	0.63 ± 0.03/0.98 ± 0.05	3.02 ± 0.15/5.36 ± 0.27	16.99 ± 0.85/18.73 ± 0.94	19.53 ± 0.98/18.26 ± 0.91	16/18	19
		π^+	79 ± 5/85 ± 4	0.18 ± 0.01/0.21 ± 0.01	1.04 ± 0.01/1.06 ± 0.01	0.63 ± 0.02/0.97 ± 0.05	3.10 ± 0.15/5.36 ± 0.27	16.99 ± 0.85/18.73 ± 0.94	18.42 ± 0.92/18.26 ± 0.91	30/23	19
	200	π^-	80 ± 5/86 ± 4	0.19 ± 0.01/0.23 ± 0.01	1.02 ± 0.01/1.06 ± 0.01	0.59 ± 0.02/0.95 ± 0.05	3.53 ± 0.17/5.99 ± 0.30	16.68 ± 0.84/18.23 ± 0.91	24.48 ± 1.22/23.86 ± 1.19	39/24	20
		π^+	80 ± 5/86 ± 4	0.19 ± 0.01/0.23 ± 0.01	1.02 ± 0.01/1.06 ± 0.01	0.59 ± 0.03/0.95 ± 0.05	3.53 ± 0.17/6.09 ± 0.30	16.68 ± 0.84/18.23 ± 0.91	25.07 ± 1.25/24.49 ± 1.22	45/68	20
STAR	200	π^-	79 ± 5/85 ± 4	0.19 ± 0.01/0.23 ± 0.01	1.04 ± 0.01/1.05 ± 0.01	0.62 ± 0.03/0.95 ± 0.05	3.70 ± 0.18/5.89 ± 0.29	16.68 ± 0.82/18.43 ± 0.92	0.26 ± 0.01/0.26 ± 0.01	22/39	5
		π^+	79 ± 4/85 ± 4	0.19 ± 0.01/0.23 ± 0.01	1.04 ± 0.01/1.05 ± 0.01	0.62 ± 0.02/0.95 ± 0.05	3.70 ± 0.18/5.89 ± 0.29	16.68 ± 0.82/18.43 ± 0.92	0.27 ± 0.01/0.26 ± 0.01	15/28	5
ALICE	900	π^-	81 ± 5/86 ± 4	0.20 ± 0.01/0.25 ± 0.01	1.03 ± 0.01/1.06 ± 0.01	0.53 ± 0.02/0.93 ± 0.05	3.63 ± 0.19/6.39 ± 0.32	16.68 ± 0.81/18.03 ± 0.90	1.47 ± 0.07/1.47 ± 0.07	34/419	26
		π^+	80 ± 3/86 ± 4	0.20 ± 0.01/0.25 ± 0.01	1.03 ± 0.01/1.06 ± 0.01	0.53 ± 0.03/0.93 ± 0.05	3.64 ± 0.19/6.39 ± 0.32	16.68 ± 0.81/18.03 ± 0.90	1.50 ± 0.08/1.50 ± 0.08	51/558	26
CMS	900	π^-	81 ± 3/87 ± 4	0.19 ± 0.01/0.25 ± 0.01	1.02 ± 0.01/1.05 ± 0.01	0.51 ± 0.03/0.89 ± 0.05	3.74 ± 0.19/6.79 ± 0.34	16.68 ± 0.80/17.83 ± 0.89	3.67 ± 0.18/3.45 ± 0.17	8/124	15
		π^+	80 ± 4/87 ± 4	0.19 ± 0.01/0.25 ± 0.01	1.02 ± 0.01/1.05 ± 0.01	0.51 ± 0.02/0.89 ± 0.05	3.72 ± 0.19/6.79 ± 0.34	16.68 ± 0.80/17.83 ± 0.89	3.74 ± 0.19/3.59 ± 0.18	6/121	15
	2760	π^-	81 ± 5/88 ± 4	0.21 ± 0.01/0.26 ± 0.01	1.02 ± 0.01/1.05 ± 0.01	0.49 ± 0.02/0.86 ± 0.05	3.96 ± 0.20/7.49 ± 0.37	16.56 ± 0.80/17.47 ± 0.87	4.46 ± 0.22/4.24 ± 0.21	15/114	15
		π^+	81 ± 5/88 ± 4	0.21 ± 0.01/0.26 ± 0.01	1.02 ± 0.01/1.05 ± 0.01	0.49 ± 0.03/0.86 ± 0.05	3.92 ± 0.20/7.49 ± 0.37	16.55 ± 0.80/17.47 ± 0.87	4.56 ± 0.23/4.44 ± 0.22	15/115	15
	7000	π^-	83 ± 4/89 ± 4	0.21 ± 0.01/0.27 ± 0.01	1.02 ± 0.01/1.05 ± 0.01	0.47 ± 0.02/0.84 ± 0.05	3.98 ± 0.19/7.69 ± 0.38	16.30 ± 0.81/17.37 ± 0.87	5.55 ± 0.28/5.41 ± 0.27	23/129	15
		π^+	82 ± 4/87 ± 4	0.21 ± 0.01/0.26 ± 0.01	1.02 ± 0.01/1.05 ± 0.01	0.47 ± 0.03/0.84 ± 0.05	3.99 ± 0.19/7.59 ± 0.38	16.37 ± 0.81/17.37 ± 0.87	5.60 ± 0.28/5.60 ± 0.28	31/171	15
	13000	π^-	83 ± 5/88 ± 4	0.22 ± 0.01/0.27 ± 0.01	1.02 ± 0.01/1.05 ± 0.01	0.46 ± 0.02/0.82 ± 0.05	4.05 ± 0.20/7.89 ± 0.39	16.31 ± 0.82/17.27 ± 0.86	5.20 ± 0.26/5.10 ± 0.26	13/50	15
		π^+	84 ± 5/86 ± 4	0.23 ± 0.01/0.27 ± 0.01	1.02 ± 0.01/1.05 ± 0.01	0.47 ± 0.03/0.80 ± 0.05	4.09 ± 0.20/7.99 ± 0.40	16.28 ± 0.82/17.07 ± 0.85	5.20 ± 0.26/5.10 ± 0.26	27/74	15

where in panel (a) only the spectra of π^- are available, and panel (c) is for NSD events and other panels are for INEL events. In some cases, different amounts marked in the panels are used to scale the data for clarity. We have fitted the data by two sets of parameter values in Eq. (7) so that we can see the fluctuations of parameter values. The blue solid (dotted) curves are our results for π^- (π^+) spectra fitted by Eq. (7) through Eqs. (1) and (3), and the blue dashed (dot-dashed) curves are our results for π^- (π^+) spectra fitted by Eq. (7) through Eqs. (2) and (3), by the first set of parameter values. The black curves are our results fitted by the second set of parameter values for comparison. The values of free parameters (T_0 , β_T , q if available, k , p_0 , and n), normalization constant (N_0), χ^2 , and degrees of freedom (dof) corresponding to the curves in Fig. 1 are listed in Tables 1 and 2. The parameter values presented in terms of value₁/value₂ denote respectively the first and second sets of parameter values in Eq. (7) through Eqs. (1) [Eqs. (2)] and (3) in which $k \neq 1$. One can see that Eq. (7) with two sets of parameter values describes the p_T spectra at mid-(pseudo)rapidity in pp collisions over an energy range from a few GeV to above 10 TeV. The blast-wave model with Boltzmann-Gibbs statistics and with Tsallis statistics presents similar results. The free parameters show some laws in the considered energy range. For a given parameter, its fluctuation at given energy is obvious in some cases.

To see clearly the excitation functions of free parameters, Figures 2(a)–2(e) show the dependences of T_0 , β_T , p_0 , n , and k on \sqrt{s} , respectively. The closed and open symbols represent the parameter values corresponding to π^- and π^+ respectively, which are listed in Tables 1 and 2. The circles (squares) represent the first set of parameter values obtained from Eq. (7) through Eqs. (1) [Eqs. (2)] and (3). The asterisks (triangles) represent the second set of parameter values obtained from Eq. (7) through Eqs. (1) [Eqs. (2)] and (3). One can see that the difference between the results of π^- and π^+ is not obvious. In the excitation functions of the first set of T_0 and β_T obtained from the blast-wave model with Boltzmann-Gibbs statistics, there are a hill at $\sqrt{s} \approx 10$ GeV, a drop at dozens of GeV, and then an increase from dozens of GeV to above 10 TeV. In the excitation functions of the first set of T_0 and β_T obtained from the blast-wave model with Tsallis statistics, there is no the complex structure, but a very low hill. In the excitation functions of the second set of T_0 and β_T , there is a slight increase from a few GeV to above 10 TeV. In Eq. (7) contained the blast-wave model with both statistics, in the excitation functions of p_0 and n , there are a slight decrease and increase respectively in the case of the hard component being available. The excitation function of k shows that the contribution $(1 - k)$ of hard component

slightly increases from dozens of GeV to above 10 TeV, and it has no contribution at around 10 GeV. At given energies, the fluctuations in a given parameter result in different excitation functions due to different selections.

Indeed, $\sqrt{s_{NN}} \approx 10$ GeV is a special energy for nucleus-nucleus collisions as indicated by Cleymans [43]. The present work shows that $\sqrt{s} \approx 10$ GeV is also a special energy for pp collisions. In particular, there is a hill in the excitation functions of T_0 and β_T in pp collisions due to a given selection of the parameters. At this energy (11 GeV more specifically [43]), the final state has the highest net baryon density, a transition from a baryon-dominated to a meson-dominated final state takes place, and the ratios of strange particles to mesons show clear and pronounced maximums [43]. These properties result in this special energy.

At 11 GeV, the chemical freeze-out temperature in nucleus-nucleus collisions is about 151 MeV [43], and the present work shows that the kinetic freeze-out temperature in pp collisions is about 105 MeV, extracted from the blast-wave model with Boltzmann-Gibbs statistics. If we do not consider the difference between nucleus-nucleus and pp collisions, though cold nuclear effect exists in nucleus-nucleus collisions, the chemical freeze-out happens obviously earlier than the kinetic one. According to an ideal fluid consideration, the time evolution of temperature follows $T_f = T_i(\tau_i/\tau_f)^{1/3}$, where T_i ($= 300$ MeV) and τ_i ($= 1$ fm) are the initial temperature and proper time respectively [44, 45], and T_f and τ_f denote the final temperature and time respectively, the chemical and kinetic freeze-outs happen at 7.8 and 23.3 fm respectively.

Strictly, T_0 (β_T) obtained from the pion spectra in the present work is less than that averaged by weighting the yields of pions, kaons, protons, and other light particles. Fortunately, the fraction of the pion yield in high energy collisions are major ($\sim 85\%$). The parameters and their tendencies obtained from the pion spectra are similar to those obtained from the spectra of all light particles. To study the excitation functions of T_0 and β_T , it does not matter if we use the spectra of pions instead of all light particles.

It should be noted that the main parameters T_0 and β_T get entangled in some way. Although the excitation functions of T_0 (β_T) which are acceptable in the fit process are not sole, their tendencies are harmonious in most cases, in particular in the energy range from the RHIC to LHC. Combining with our previous work [18], we could say that there is a slight ($\sim 10\%$) increase in the excitation function of T_0 and an obvious ($\sim 35\%$) increase in the excitation function of β_T from the RHIC to LHC. At least, the excitation functions of T_0 and β_T do not decrease from the RHIC to LHC.

However, the excitation functions of T_0 and β_T from

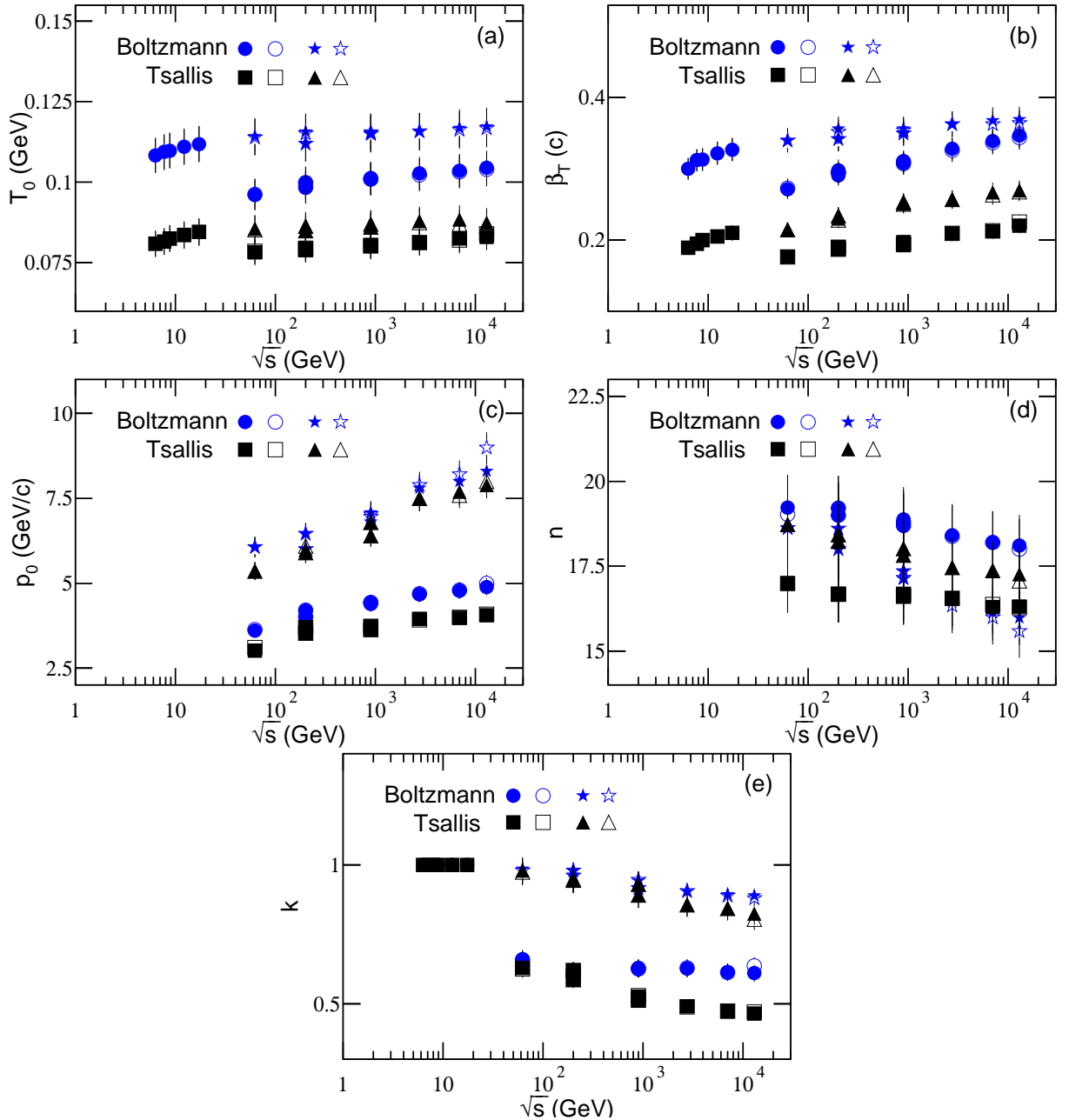


Fig. 2. Excitation functions of (a) T_0 , (b) β_T , (c) p_0 , (d) n , and (e) k . The closed (open) symbols represent the parameter values corresponding to π^- (π^+) spectra, which are listed in Tables 1 and 2. The circles (squares) represent the first set of parameter values obtained from Eq. (7) through Eqs. (1) [Eqs. (2) and (3)]. The asterisks (triangles) represent the second set of parameter values obtained from Eq. (7) through Eqs. (1) [Eqs. (2) and (3)]. The related parameter values are listed in Tables 1 and 2.

low to high energies are not always incremental or invariant. For example, In ref. [4], T_0 slowly decreases as \sqrt{s} increases from 23 GeV to 1.8 TeV, and β_T slowly increases with \sqrt{s} . In refs. [19, 20], T_0 has no obvious change and β_T has a slight ($\sim 10\%$) increase from the RHIC to LHC. In ref. [21], T_0 has a slight ($\sim 9\%$) increase and β_T has a large ($\sim 65\%$) increase from the

RHIC to LHC. In ref. [22, 23], T_0 has a slight ($\sim 5\%$) decrease from the RHIC to LHC and β_T increases by $\sim 20\%$ from 39 to 200 GeV. It is convinced that β_T increases from the RHIC to LHC, though the situation of T_0 is doubtful.

Although some works [46–49] reported a decrease of T_0 and an increase of β_T from the RHIC to LHC, our

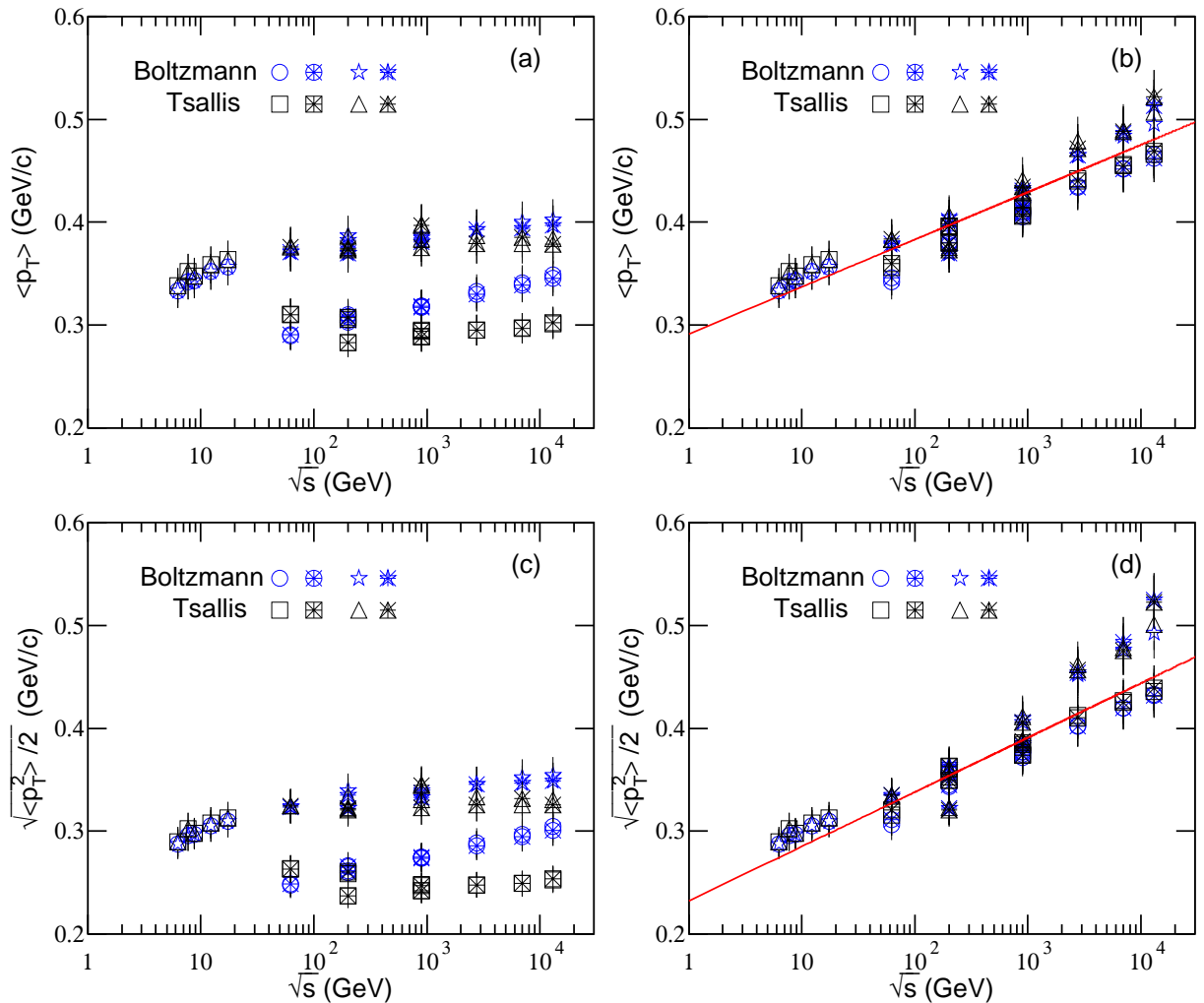


Fig. 3. Excitation functions of (a)(b) $\langle p_T \rangle$ and (c)(d) $\sqrt{\langle p_T^2 \rangle}/2$. The open symbols (open symbols with asterisks) represent the values corresponding to π^- (π^+) spectra. The circles (squares) represent the results obtained indirectly from Eq. (1) [Eq. (2)] for the left panel, or from Eq. (7) through Eqs. (1) [Eqs. (2)] and (3) for the right panel, by the first set of parameter values. The results by the second set of parameter values are presented by the asterisks (triangles). These values are indirectly obtained according to the parameter values listed in Tables 1 and 2. The lines are the fitted results for various symbols.

re-scans on their plots show a different situation of T_0 . For example, in ref. [46], our re-scans show that T_0 has no obvious change and β_T has a slight ($\sim 9\%$) increase from the RHIC to LHC, though there is an obvious hill or there is an increase by $\sim 30\%$ in T_0 in 5–40 GeV comparing with that at the RHIC. Ref. [47] shows similar results to ref. [46] with the almost invariant T_0 from the top RHIC to LHC, an increase by $\sim 28\%$ in T_0 in 7–40 GeV comparing with that at the top RHIC, and an increase by $\sim 8\%$ in β_T comparing with that at the top RHIC. Refs. [48, 49] shows similar result to refs. [46, 47] on T_0 , though the excitation function of β_T is

not available.

In most cases, the correlation between T_0 and β_T are not negative, though some works [46, 47] show negative correlation over a wide energy range. For a give p_T spectrum, it seems that a larger T_0 corresponds to a smaller β_T , which shows a negative correlation. However, this negative correlation is not sole case. In fact, a couple of suitable T_0 and β_T can fit a give p_T spectrum. A series of p_T spectra at different energies possibly show a positive correlation between T_0 and β_T , or independent of T_0 on β_T , in a narrow energy range.

Table 3. Values of T_0 , β_T , k , p_0 , n , N_0 , χ^2 , and dof corresponding to the solid (dotted) curves for π^- (π^+) spectra in Fig. 4.

Collab.	\sqrt{s} (GeV)	Part.	T_0 (MeV)	β_T (c)	k	p_0 (GeV/c)	n	N_0	χ^2	dof
NA61/	6.3	π^-	105 ± 5	0.31 ± 0.02	1	—	—	0.08 ± 0.01	24	15
SHINE	7.7	π^-	106 ± 5	0.32 ± 0.02	1	—	—	0.10 ± 0.01	44	15
	8.8	π^-	107 ± 5	0.32 ± 0.02	1	—	—	0.10 ± 0.01	86	15
	12.3	π^-	108 ± 5	0.33 ± 0.02	1	—	—	0.12 ± 0.01	78	15
	17.3	π^-	109 ± 5	0.33 ± 0.02	1	—	—	0.13 ± 0.01	34	15
PHENIX	62.4	π^-	111 ± 5	0.35 ± 0.02	0.99 ± 0.01	3.58 ± 0.18	19.26 ± 0.56	19.48 ± 0.97	9	20
		π^+	111 ± 5	0.35 ± 0.02	0.99 ± 0.01	3.59 ± 0.18	19.26 ± 0.56	19.54 ± 0.97	18	20
	200	π^-	115 ± 6	0.37 ± 0.02	0.99 ± 0.02	4.20 ± 0.21	18.71 ± 0.54	24.11 ± 1.20	16	21
		π^+	115 ± 6	0.36 ± 0.02	0.99 ± 0.02	4.31 ± 0.22	18.61 ± 0.53	24.96 ± 1.22	26	21
STAR	200	π^-	114 ± 6	0.34 ± 0.02	1	—	—	0.26 ± 0.01	2	6
		π^+	114 ± 6	0.34 ± 0.02	1	—	—	0.27 ± 0.01	6	6
ALICE	900	π^-	118 ± 5	0.35 ± 0.02	0.95 ± 0.02	4.41 ± 0.22	18.67 ± 0.53	3.70 ± 0.18	101	27
		π^+	118 ± 5	0.35 ± 0.02	0.95 ± 0.02	4.40 ± 0.22	18.67 ± 0.53	3.69 ± 0.18	131	27
CMS	900	π^-	118 ± 6	0.35 ± 0.02	0.91 ± 0.02	4.03 ± 0.20	18.87 ± 0.54	8.90 ± 0.44	47	16
		π^+	118 ± 5	0.35 ± 0.02	0.91 ± 0.02	4.00 ± 0.20	18.67 ± 0.55	9.03 ± 0.45	43	16
	2760	π^-	122 ± 6	0.36 ± 0.02	0.89 ± 0.02	4.01 ± 0.18	18.80 ± 0.54	11.34 ± 0.57	57	16
		π^+	122 ± 6	0.37 ± 0.02	0.89 ± 0.02	4.02 ± 0.18	18.57 ± 0.53	11.54 ± 0.58	76	16
	7000	π^-	123 ± 6	0.38 ± 0.02	0.87 ± 0.02	4.03 ± 0.18	18.50 ± 0.52	14.50 ± 0.73	73	16
		π^+	123 ± 6	0.38 ± 0.02	0.86 ± 0.02	4.03 ± 0.18	18.40 ± 0.52	14.66 ± 0.73	90	16
	13000	π^-	126 ± 6	0.37 ± 0.02	0.83 ± 0.02	4.04 ± 0.19	18.30 ± 0.51	13.62 ± 0.68	31	16
		π^+	126 ± 6	0.37 ± 0.02	0.83 ± 0.02	4.04 ± 0.19	18.30 ± 0.51	13.84 ± 0.69	57	16

Table 4. Values of T_0 , β_T , q , k , p_0 , n , N_0 , χ^2 , and dof corresponding to the dashed (dot-dashed) curves for π^- (π^+) spectra in Fig. 4.

Collab.	\sqrt{s} (GeV)	Part.	T_0 (MeV)	β_T (c)	q	k	p_0 (GeV/c)	n	N_0	χ^2	dof
NA61/	6.3	π^-	83 ± 5	0.24 ± 0.01	1.04 ± 0.01	1	—	—	0.09 ± 0.01	11	14
SHINE	7.7	π^-	84 ± 5	0.25 ± 0.02	1.04 ± 0.01	1	—	—	0.10 ± 0.01	8	14
	8.8	π^-	84 ± 5	0.25 ± 0.01	1.04 ± 0.01	1	—	—	0.10 ± 0.01	23	14
	12.3	π^-	85 ± 5	0.26 ± 0.01	1.05 ± 0.01	1	—	—	0.12 ± 0.01	11	14
	17.3	π^-	86 ± 5	0.26 ± 0.01	1.05 ± 0.01	1	—	—	0.13 ± 0.01	4	14
PHENIX	62.4	π^-	$82 \pm 4/88 \pm 4$	$0.24 \pm 0.01/0.27 \pm 0.01$	$1.07 \pm 0.01/1.05 \pm 0.01$	$0.99 \pm 0.01/0.99 \pm 0.01$	$3.20 \pm 0.19/3.19 \pm 0.18$	$18.56 \pm 0.51/18.56 \pm 0.51$	$18.27 \pm 0.91/19.18 \pm 0.93$	33/39	18
		π^+	$82 \pm 5/88 \pm 4$	$0.24 \pm 0.01/0.27 \pm 0.01$	$1.07 \pm 0.01/1.06 \pm 0.01$	$0.99 \pm 0.01/0.99 \pm 0.01$	$3.20 \pm 0.19/3.21 \pm 0.18$	$18.56 \pm 0.51/18.56 \pm 0.51$	$17.19 \pm 0.89/17.36 \pm 0.90$	15/15	18
	200	π^-	$83 \pm 5/90 \pm 4$	$0.25 \pm 0.02/0.28 \pm 0.01$	$1.07 \pm 0.01/1.06 \pm 0.01$	$0.99 \pm 0.01/0.99 \pm 0.01$	$3.99 \pm 0.19/3.89 \pm 0.19$	$18.06 \pm 0.51/18.06 \pm 0.51$	$23.21 \pm 1.15/22.40 \pm 1.10$	16/31	19
		π^+	$83 \pm 5/90 \pm 4$	$0.25 \pm 0.02/0.28 \pm 0.01$	$1.07 \pm 0.01/1.06 \pm 0.01$	$0.99 \pm 0.01/0.99 \pm 0.01$	$4.09 \pm 0.20/4.09 \pm 0.20$	$18.01 \pm 0.50/18.01 \pm 0.51$	$23.00 \pm 1.16/22.40 \pm 1.14$	26/32	19
STAR	200	π^-	$83 \pm 5/89 \pm 4$	$0.25 \pm 0.01/0.28 \pm 0.01$	$1.06 \pm 0.01/1.04 \pm 0.01$	1	—	—	0.26 ± 0.01	34	5
		π^+	$83 \pm 5/89 \pm 4$	$0.25 \pm 0.01/0.28 \pm 0.01$	$1.06 \pm 0.01/1.04 \pm 0.01$	1	—	—	0.26 ± 0.01	38	5
ALICE	900	π^-	$84 \pm 5/91 \pm 4$	$0.26 \pm 0.01/0.30 \pm 0.01$	$1.06 \pm 0.01/1.03 \pm 0.01$	$0.94 \pm 0.02/0.94 \pm 0.02$	$4.11 \pm 0.19/4.11 \pm 0.19$	$17.99 \pm 0.50/17.99 \pm 0.50$	$0.59 \pm 0.02/0.58 \pm 0.02$	187/287	25
		π^+	$85 \pm 4/91 \pm 4$	$0.26 \pm 0.01/0.30 \pm 0.01$	$1.06 \pm 0.01/1.03 \pm 0.01$	$0.94 \pm 0.02/0.94 \pm 0.02$	$4.11 \pm 0.20/4.11 \pm 0.20$	$17.99 \pm 0.40/17.99 \pm 0.40$	$0.59 \pm 0.02/0.58 \pm 0.02$	232/333	25
CMS	900	π^-	$87 \pm 4/92 \pm 4$	$0.27 \pm 0.01/0.30 \pm 0.01$	$1.05 \pm 0.01/1.03 \pm 0.01$	$0.88 \pm 0.02/0.87 \pm 0.02$	$3.85 \pm 0.19/3.85 \pm 0.19$	$18.40 \pm 0.51/18.40 \pm 0.51$	$1.43 \pm 0.26/1.42 \pm 0.27$	79/95	14
		π^+	$87 \pm 4/93 \pm 4$	$0.27 \pm 0.01/0.30 \pm 0.01$	$1.05 \pm 0.01/1.03 \pm 0.01$	$0.89 \pm 0.02/0.86 \pm 0.02$	$3.82 \pm 0.19/3.61 \pm 0.19$	$18.53 \pm 0.51/18.53 \pm 0.51$	$1.42 \pm 0.25/1.42 \pm 0.24$	84/72	14
	2760	π^-	$89 \pm 5/93 \pm 5$	$0.28 \pm 0.01/0.30 \pm 0.02$	$1.05 \pm 0.01/1.03 \pm 0.01$	$0.85 \pm 0.02/0.83 \pm 0.02$	$3.92 \pm 0.20/3.92 \pm 0.20$	$18.43 \pm 0.52/18.43 \pm 0.52$	$1.67 \pm 0.27/1.81 \pm 0.27$	84/72	14
		π^+	$89 \pm 5/93 \pm 5$	$0.28 \pm 0.02/0.30 \pm 0.02$	$1.05 \pm 0.01/1.03 \pm 0.01$	$0.85 \pm 0.02/0.84 \pm 0.02$	$3.92 \pm 0.20/3.92 \pm 0.20$	$18.43 \pm 0.51/18.43 \pm 0.51$	$1.83 \pm 0.27/1.82 \pm 0.26$	102/88	14
	7000	π^-	$90 \pm 4/94 \pm 5$	$0.29 \pm 0.02/0.31 \pm 0.02$	$1.05 \pm 0.01/1.03 \pm 0.01$	$0.84 \pm 0.02/0.81 \pm 0.02$	$3.94 \pm 0.19/3.94 \pm 0.19$	$18.41 \pm 0.50/18.41 \pm 0.50$	$2.30 \pm 0.32/2.30 \pm 0.33$	103/69	14
		π^+	$90 \pm 4/94 \pm 5$	$0.29 \pm 0.01/0.31 \pm 0.02$	$1.05 \pm 0.01/1.03 \pm 0.01$	$0.83 \pm 0.02/0.81 \pm 0.02$	$3.95 \pm 0.20/3.95 \pm 0.20$	$18.41 \pm 0.50/18.41 \pm 0.50$	$2.31 \pm 0.33/2.30 \pm 0.32$	124/92	14
	13000	π^-	$91 \pm 5/95 \pm 5$	$0.30 \pm 0.01/0.31 \pm 0.02$	$1.05 \pm 0.01/1.02 \pm 0.01$	$0.82 \pm 0.02/0.80 \pm 0.02$	$3.96 \pm 0.19/3.96 \pm 0.19$	$18.31 \pm 0.41/18.31 \pm 0.41$	$2.19 \pm 0.39/2.17 \pm 0.38$	55/39	14
		π^+	$90 \pm 5/95 \pm 5$	$0.30 \pm 0.01/0.31 \pm 0.02$	$1.05 \pm 0.01/1.02 \pm 0.01$	$0.82 \pm 0.02/0.79 \pm 0.02$	$3.96 \pm 0.19/3.96 \pm 0.19$	$18.31 \pm 0.41/18.31 \pm 0.41$	$2.18 \pm 0.38/2.17 \pm 0.36$	92/59	14

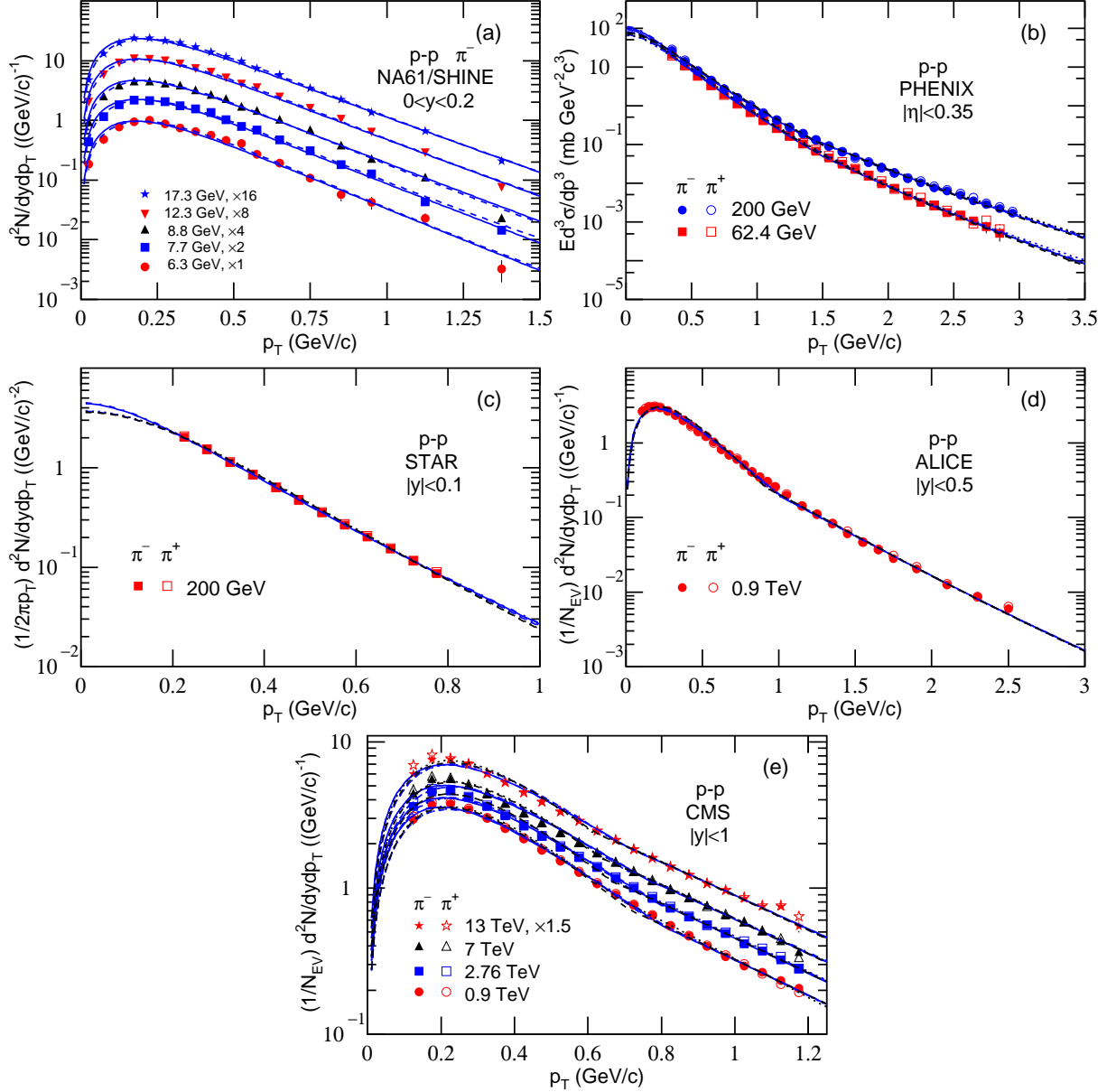


Fig. 4. Same as Fig. 1, but showing the results fitted by Eq. (8) through Eqs. (1) and (3) with one set of parameter values and by Eq. (8) through Eqs. (2) and (3) with two sets of parameter values. The blue solid (dotted) curves are the results for π^- (π^+) spectra fitted by Eq. (8) through Eqs. (1) and (3), and the blue and black dashed (dot-dashed) curves are the results for π^- (π^+) spectra fitted by Eq. (8) through Eqs. (2) and (3).

To study further the behaviors of parameters, Figure 3 shows the excitation functions of (a)(b) mean p_T ($\langle p_T \rangle$) and (c)(d) ratio of root-mean-square p_T ($\sqrt{\langle p_T^2 \rangle}$) to $\sqrt{2}$, where the left panel [(a)(c)] corresponds to the results of the first component [Eq. (1) or (2)] and the right panel [(b)(d)] corresponds to the results of the two components [Eq. (7)]. The open symbols (open symbols with asterisks) represent the values corresponding to π^- (π^+) spectra. The circles (squares) represent the values obtained indirectly from Eq. (1) [Eq. (2)] for the left

panel or Eq. (7) through Eqs. (1) [Eqs. (2)] and (3) for the right panel, by the first set of parameter values. The results by the second set of parameter values are presented by the asterisks (triangles). These values are indirectly obtained from the equations according to the parameters listed in Tables 1 and 2 over a p_T range from 0 to 5 GeV/c which is beyond the available range of the data. If the initial temperature of interacting system is approximately presented by $T_i = \sqrt{\langle p_T^2 \rangle}/2$ [50–52], the lower panel shows the excitation function of initial tem-

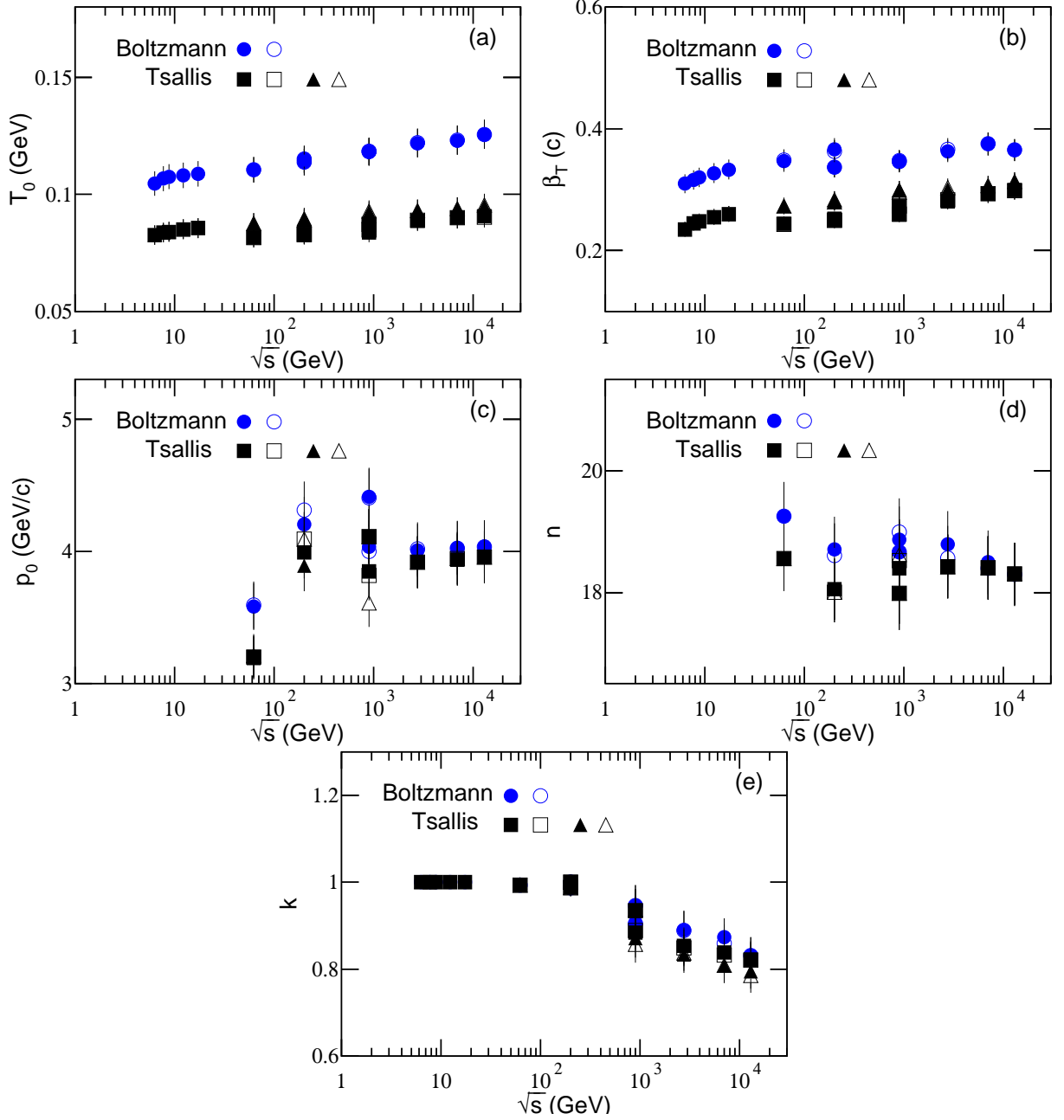


Fig. 5. Same as Fig. 2, but showing the results obtained from Eq. (8) through Eqs. (1) and (3) with one set of parameter values and from Eq. (8) through Eqs. (2) and (3) with two sets of parameter values. The circles represent the parameter values obtained from Eq. (8) through Eqs. (1) and (3). The squares (triangles) represent the first (second) set of parameter values obtained from Eq. (8) through Eqs. (2) and (3). The related parameter values are listed in Tables 3 and 4.

perature. It should be noted that the root-mean square momentum component of particles in the rest frame of isotropic emission source is regarded as the initial temperature, or at the least it is a reflection of the initial temperature. The relations in the left panel are complex and multiple due to different sets of parameter values. The lines in the right panel are fitted to various symbols

by linear functions

$$\langle p_T \rangle = (0.291 \pm 0.006) + (0.020 \pm 0.001) \ln \sqrt{s} \quad (11)$$

and

$$T_i = (0.232 \pm 0.008) + (0.023 \pm 0.002) \ln \sqrt{s} \quad (12)$$

with $\chi^2/\text{dof}=54/82$ and $107/82$ respectively. One can see that the behaviors of $\langle p_T \rangle$ and T_i are very similar to

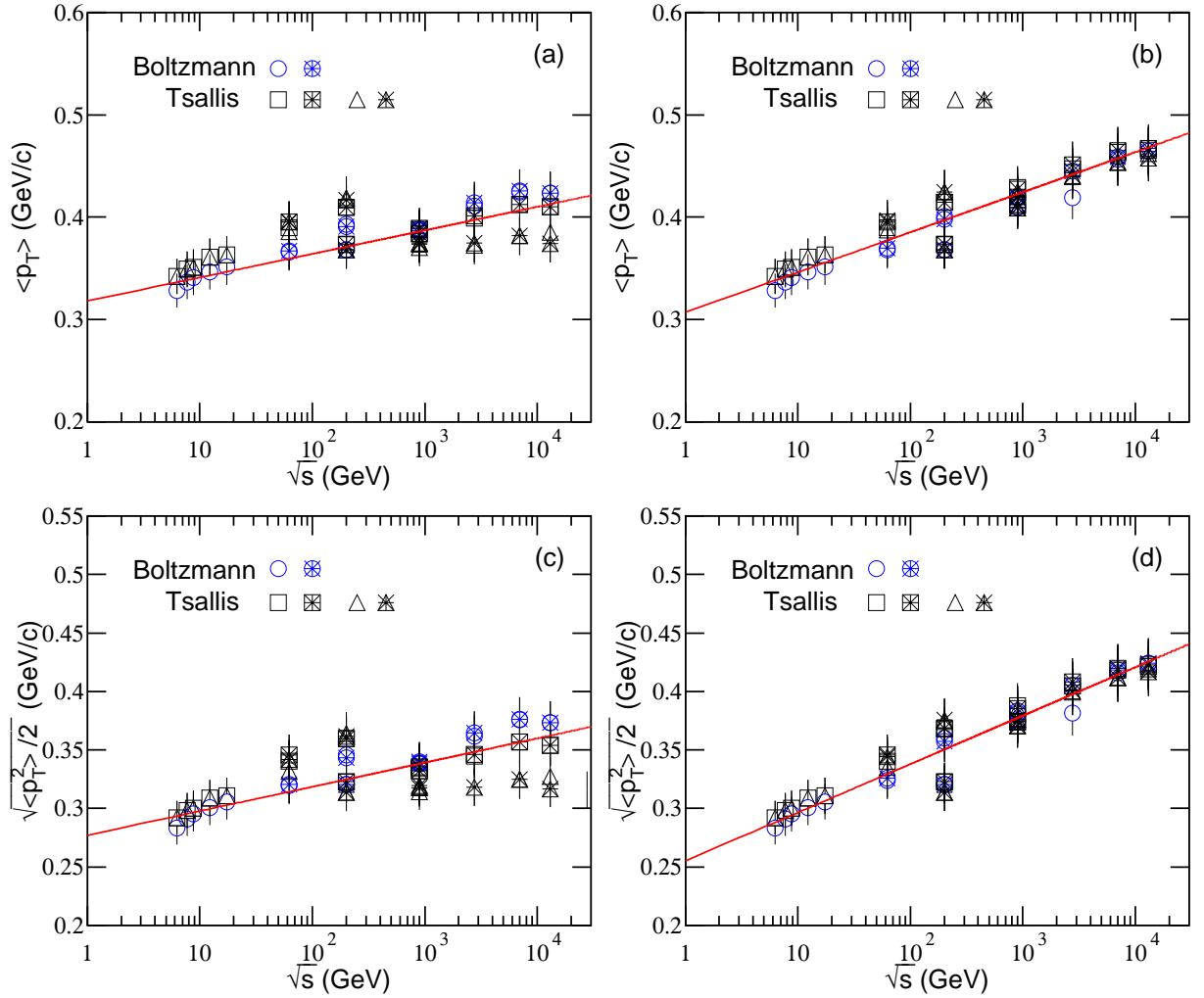


Fig. 6. Same as Fig. 3, but showing the results obtained from Eq. (1) [Eq. (2)] for the left panel, or from Eq. (8) through Eqs. (1) [Eqs. (2)] and (3) for the right panel. The circles represent the results obtained indirectly from Eq. (1) for the left panel, or from Eq. (8) through Eqs. (1) and (3) for the right panel, by the parameter values. The squares (triangles) represent the results obtained indirectly from Eq. (2) for the left panel, or from Eq. (8) through Eqs. (2) and (3) for the right panel, by the first (second) set of parameter values. These values are indirectly obtained according to the parameter values listed in Tables 3 and 4.

each other. In particular, with the increase of $\ln \sqrt{s}$ and including the contribution of second component, $\langle p_T \rangle$ and T_i increase approximately linearly.

The quantities $\langle p_T \rangle$ and T_i are very important to understand the excitation degree of interacting system. As for the right panel in Fig. 3 which is for the two-component, the incremental trend for $\langle p_T \rangle$ and T_i with the increase of \sqrt{s} is a natural result due to more energy deposition at higher energy. Although $\langle p_T \rangle$ and T_i are obtained from the parameter values listed in Tables 1 and 2, they are independent of models. More investigations on the excitation functions of $\langle p_T \rangle$ and T_i are needed due to their importance.

To discuss further, for comparisons with the results from Eq. (7), we reanalyze the spectra by Eq. (8) and

study the trends of new parameters. Figure 4 is the same as Fig. 1, but showing the results fitted by Eq. (8) through Eqs. (1) and (3) and through Eqs. (2) and (3) respectively. For Eq. (8) through Eqs. (1) and (3), only one set of parameter values are used due to the fact that there is no entanglement in the extraction of parameters in the two-component model. For Eq. (8) through Eqs. (2) and (3), two sets of parameter values are used due to the fact that q affects the extraction of other parameters in the two-component model. The values of related parameters are listed in Tables 3 and 4 which are the same as Tables 1 and 2 respectively, and with only one set of parameter values in Table 3. The related parameters are shown in Fig. 5 and the leading-out parameters are shown in Fig. 6, which are

the same as Figs. 2 and 3 respectively, and with only one set of parameter values for Eq. (8) through Eqs. (1) and (3). In particular, k in Fig. 5 is obtained by $k = \int_0^{p_1} A_1 f_S(p_T) dp_T$ due to $f_0(p_T)$ is normalized to 1. The lines in Fig. 6 are fitted by linear functions

$$\langle p_T \rangle = (0.318 \pm 0.004) + (0.010 \pm 0.001) \ln \sqrt{s} \quad (13)$$

and

$$T_i = (0.277 \pm 0.004) + (0.009 \pm 0.001) \ln \sqrt{s} \quad (14)$$

with $\chi^2/\text{dof}=55/61$ and $72/61$ respectively for the left panel, and

$$\langle p_T \rangle = (0.307 \pm 0.005) + (0.017 \pm 0.001) \ln \sqrt{s} \quad (15)$$

and

$$T_i = (0.255 \pm 0.005) + (0.018 \pm 0.001) \ln \sqrt{s} \quad (16)$$

with $\chi^2/\text{dof}=28/61$ and $37/61$ respectively for the right panel, though the linear relationships between the parameters and $\ln \sqrt{s}$ may be not the best fitting functions.

One can see that Eq. (8) fits similarly good the data as Eq. (7). T_0 and β_T in Fig. 5 increase slightly from a few GeV to above 10 TeV with some fluctuations in some cases, which is partly similar to those in Fig. 2. Other parameters in Fig. 5 show somehow similar trends to Fig. 2 with some differences. The left panels in Figs. 6 and 3 are different due to the first component being in different superpositions. The right panels in Figs. 6 and 3 are very similar to each other due to the same data sets being fitted.

Combining with our recent work [53], it is shown the similarity in pp and nucleus-nucleus collisions. Moreover, it is well seen that Tsallis does not distinguish well between the data in pp and nucleus-nucleus collisions [54–56]. Concerning around 10–20 GeV change, this is expected as soon as QCD effects/calculations may not be directly applicable below this point, plus seem to be smoothed away by other processes in nucleus-nucleus collisions. This is well visible as a clear difference as shown in refs. [54–56], where the data in pp collisions goes well with the data in electron-positron collisions, while the data in nucleus-nucleus collisions are different.

The differences between Eqs. (7) and (8) are obviously, though the similar components are used in them. In our recent works [18, 57], Eqs. (7) and (8) are used respectively. Although there is entanglement in the extraction of parameters, a smooth curve can be easily obtained by Eq. (7). Although it is not easy to obtain a smooth curve at the point of junction, there is no or less entanglement in the extraction of parameters by Eq. (8). In consideration of obtaining a set of parameters with least entanglement, we are inclined to use Eq. (8)

to extract the related parameters. This inclining results in Eq. (8) to separate determinedly the contributions of soft and hard processes.

4 Summary and conclusion

The transverse momentum spectra of π^- and π^+ produced at mid-(pseudo)rapidity in pp collisions over an energy range from a few GeV to above 10 TeV have been analyzed by the superposition of the blast-wave model with Boltzmann-Gibbs statistics or with Tsallis statistics and the inverse power-law (Hagedorn function). The model results are well fitting to the experimental data of NA61/SHINE, PHENIX, STAR, ALICE, and CMS Collaborations. The values of related parameters are extracted from the fit process and the excitation functions of parameters are obtained.

In the particular superposition Eq. (7) and with a given selection, both excitation functions of T_0 and β_T obtained from the blast-wave model with Boltzmann-Gibbs statistics show a hill at $\sqrt{s} \approx 10$ GeV, a drop at dozens of GeV, and an increase from dozens of GeV to above 10 TeV. The mentioned two excitation functions obtained from the blast-wave model with Tsallis statistics does not show the complex structure, but a very low hill. In another selection for the parameters in Eq. (7) or in the superposition Eq. (8), T_0 and β_T increase generally slightly from a few GeV to above 10 TeV with some fluctuations in some cases. In both superpositions, the excitation function of p_0 (n) shows a slight decrease (increase) in the case of the hard component being available. From the RHIC to LHC, there is a positive (negative) correlation between T_0 and β_T (p_0 and n). The contribution of hard component slightly increases from dozens of GeV to above 10 TeV, and it has no contribution at around 10 GeV.

In the case of considering the two components together, the mean transverse momentum and the initial temperature increase approximately linearly with the increase of logarithmic collision energy. From a few GeV to above 10 TeV, the collision system takes place possibly two main transitions. At around 10 GeV, a transition from a baryon-dominated to a meson-dominated intermediate and final states takes place. From dozens of GeV to above 10 TeV, a transition from a meson-dominated to a parton-dominated intermediate state takes place, though both final states are meson-dominated. It is a long-term target to search for the critical energy at which a parton-dominated intermediate state appears initially.

Data Availability

The data used to support the findings of this study

are quoted from the mentioned references. As a phenomenological work, this paper does not report new data.

Conflicts of Interest

The authors declare that there are no conflicts of interest regarding the publication of this paper.

Acknowledgments

Communications from Edward K. Sarkisyan-Grinbaum are highly acknowledged. This work was supported by the National Natural Science Foundation of China under Grant Nos. 11575103 and 11747319, the Shanxi Provincial Natural Science Foundation under Grant No. 201701D121005, and the Fund for Shanxi “1331 Project” Key Subjects Construction.

References

- [1] Cleymans J, Oeschler H, Redlich K and Wheaton S 2006 *Phys. Rev. C* **73** 034905
- [2] Andronic A, Braun-Munzinger P and Stachel J 2009 *Acta Phys. Pol. B* **40** 1005
- [3] Andronic A, Braun-Munzinger P and Stachel J 2010 *Nucl. Phys. A* **834** 237c
- [4] Hama Y and Navarra F S 1992 *Z. Phys. C* **53** 501
- [5] Schnedermann E, Sollfrank J and Heinz U 1993 *Phys. Rev. C* **48** 2462
- [6] Abelev B I *et al* (STAR Collaboration) *Phys. Rev. C* **79** 034909
- [7] Abelev B I *et al* 2010 (STAR Collaboration) *Phys. Rev. C* **81** 024911
- [8] Tang Z B, Xu Y C, Ruan L J, van Buren G, Wang F Q and Xu Z B 2009 *Phys. Rev. C* **79** 051901(R)
- [9] Tang Z B, Li Y, Ruan L J, Shao M, Chen H F, Li C, Mohanty B, Sorensen P, Tang A H and Xu Z B 2013 *Chin. Phys. Lett.* **30** 031201
- [10] Jiang K, Zhu Y Y, Liu W T, Chen H F, Li C, Ruan L J, Tang Z B, Xu Z B 2015 *Phys. Rev. C* **91** 024910
- [11] Takeuchi S, Murase K, Hirano T, Huovinen P and Nara Y 2015 *Phys. Rev. C* **92** 044907
- [12] Heiselberg H and Levy A M 1999 *Phys. Rev. C* **59** 2716
- [13] Heinz U W 2004 *Lecture Notes for Lectures Presented at the 2nd CERN-Latin-American School of High-Energy Physics (San Miguel Regla, Mexico, 1-14 June 2003)* (arXiv:hep-ph/0407360)
- [14] Russo R 2015 Measurement of D^+ meson production in p-Pb collisions with the ALICE detector *PhD Thesis* Universita degli Studi di Torino, Italy (arXiv:1511.04380 [nucl-ex])
- [15] Wei H-R, Liu F-H and Lacey R A 2016 *Eur. Phys. J. A* **52** 102
- [16] Lao H-L, Wei H-R, Liu F-H and Lacey R A 2016 *Eur. Phys. J. A* **52** 203
- [17] Wei H-R, Liu F-H and Lacey R A 2016 *J. Phys. G* **43** 125102
- [18] Lao H-L, Liu F-H, Li B-C and Duan M-Y 2018 *Nucl. Sci. Tech.* **29** 82
- [19] Andronic A 2014 *Int. J. Mod. Phys. A* **29** 1430047
- [20] Abelev B *et al* (ALICE Collaboration) 2012 *Phys. Rev. Lett.* **109** 252301
- [21] Zhang S, Ma Y G, Chen J H and Zhong C 2015 *Adv. High Energy Phys.* **2015** 460590
- [22] Das S (for the STAR collaboration) 2015 *EPJ Web of Conf.* **90** 08007
- [23] Das S (for the STAR collaboration) 2013 *Nucl. Phys. A* **904-905** 891c
- [24] Abgrall N *et al* (NA61/SHINE Collaboration) 2014 *Eur. Phys. J. C* **74** 2794
- [25] Adare A *et al* (PHENIX Collaboration) 2011 *Phys. Rev. C* **83** 064903
- [26] Aamodt K *et al* (ALICE Collaboration) 2011 *Eur. Phys. J. C* **71** 1655
- [27] Chatrchyan S *et al* (CMS Collaboration) 2012 *Eur. Phys. J. C* **72** 2164
- [28] Sirunyan A M *et al* (CMS Collaboration) 2017 *Phys. Rev. D* **96** 112003
- [29] Cleymans J and Worku D 2012 *Eur. Phys. J. A* **48** 160
- [30] Zheng H and Zhu L L 2016 *Adv. High Energy Phys.* **2016** 9632126
- [31] Odorico R 1982 *Phys. Lett. B* **118** 151
- [32] Arnison G *et al* (UA1 Collaboration) 1982 *Phys. Lett. B* **118** 167
- [33] Mizoguchi T, Biyajima M and Suzuki N 2017 *Int. J. Mod. Phys. A* **32** 1750057
- [34] Hagedorn R 1983 *Riv. Nuovo Cimento* **6**(No. 10) 1
- [35] Abelev B *et al* (ALICE Collaboration) 2015 *Eur. Phys. J. C* **75** 1
- [36] Aamodt K *et al* (ALICE Collaboration) 2010 *Phys. Lett. B* **693** 53
- [37] Falco A D (for the ALICE collaboration) 2011 *J. Phys. G* **38** 124083
- [38] Abelev B *et al* (ALICE Collaboration) 2012 *Phys. Lett. B* **710** 557
- [39] Abt I *et al.* (HERA-B Collaboration) 2007 *Eur. Phys. J. C* **50** 315
- [40] Abelev B *et al* (ALICE Collaboration) 2012 *Phys. Lett. B* **718** 295 and Erratum 2015 *Phys. Lett. B* **748** 472
- [41] Lakomov I (for the ALICE collaboration) 2014 *Nucl. Phys. A* **931** 1179
- [42] Abelev B *et al* (ALICE Collaboration) 2012 *Phys. Lett. B* **708** 265
- [43] Cleymans J 2017 (arXiv:1711.02882 [hep-ph])
- [44] Bjorken J D 1983 *Phys. Rev. D* **27** 140
- [45] Okamoto K and Nonaka C 2017 *Eur. Phys. J. C* **77** 383
- [46] Zhang S, Ma Y G, Chen J H and Zhong C 2016 *Adv. High Energy Phys.* **2016** 9414239
- [47] Adamczyk L *et al* (STAR Collaboration) 2017 *Phys. Rev. C* **96** 044904
- [48] Luo X F 2016 *Nucl. Phys. A* **956** 75
- [49] Chatterjee S, Das S, Kumar L, Mishra D, Mohanty B, Sahoo R and Sharma N 2015 *Adv. High Energy Phys.* **2015** 349013
- [50] Gutay L G, Hirsch A S, Pajares C, Scharenberg R P and Srivastava B K 2015 *Int. J. Mod. Phys. E* **24** 1550101

- [51] Hirsch A S, Pajares C, Scharenberg R P and Srivastava B K 2018 (arXiv:1803.02301 [hep-ph])
- [52] Sahoo P, De S, Tiwari S K and Sahoo R 2018 *Eur. Phys. J. A* **54** 136
- [53] Li L-L and Liu F-H 2018 *Eur. Phys. J. A* **54** 169
- [54] Sarkisyan E K G and Sakharov A S 2004 (CERN-PH-TH-2004-213 and arXiv:hep-ph/0410324)
- [55] Sarkisyan E K G and Sakharov A S 2006 *AIP Conf. Proc.* **828** 35 (arXiv:hep-ph/0510191)
- [56] Back B B *et al* (PHOBOS Collaboration) 2006 *Phys. Rev. C* **74** 021902(R)
- [57] Lao H-L, Liu F-H, Li B-C, Duan M-Y and Lacey R A 2018 *Nucl. Sci. Tech.* **29** 164